Article

Study on Rolling Defects of Al-Mg Alloys with High Mg Content at Normal Rolling and Cross-Rolling Processes

Seong-Sik Lim , Jae-Pyo Hong , Min-Ki Kim , Young-Chul Park , Sang-Mok Lee , Dae-Yeon Cho , Chang-Hee Cho *

Posted Date: 17 July 2023

doi: 10.20944/preprints202307.1095.v1

Keywords: high Mg content Al-Mg alloy; Finite Element Analysis (FEA); electron backscattered diffraction (EBSD); cross-rolling; defect; Goss texture

Article

Study on Rolling Defects of Al-Mg Alloys with High Mg Content at Normal Rolling and Cross-Rolling Processes

Seong-Sik Lim[1], Jae-Pyo Hong[2,3], Min-Ki Kim[1], Young-Chul Park[2,4], Sang-Mok Lee[2], Dae-Yeon Cho[2], and Chang-Hee Cho[2,5]*

[1] Molding & Metal Forming R&D Department, Korea Institute of Industrial Technology, Incheon 21999, Republic of Korea; sslim@kitech.re.kr, mkim@kitech.re.kr
[2] R&D Center, RtoB Co., Ltd., Incheon 21632; hjp@rtob.co.kr, ycpark@rtob.co.kr, smlee@rtob.co.kr, cdy@rtob.co.kr, choch@rtob.co.kr
[3] Department of Mechanical Engineering, Inha University, Incheon 22212, Republic of Korea;
[4] Department of Materials Science and Engineering, Inha University, Incheon 22212, Republic of Korea;
[5] Department of Materials Science and Engineering, Northwestern University, 2220 Campus Drive, Evanston, IL 60208, United States; Chang-heeCho2028@u.northwestern.edu
* Correspondence: choch@rtob.co.kr; Chang-heeCho2028@u.northwestern.edu; (Chang-Hee Cho)

Abstract: This study investigated defect formation and strain distribution in high Mg content Al-Mg alloys during normal rolling and cross-rolling processes. The Finite Element Analysis (FEA) revealed the presence of wave defects and strain localization-induced zipper cracks in normal cold rolling, which were confirmed by experimental results. The concentration of shear strain played a significant role in crack formation and propagation. However, the influence of wave defects was minimal in the cross-rolling process, which exhibited a relatively uniform strain distribution. Nonetheless, strain concentration at the edge and center regions led to the formation of zipper cracks and edge cracks, with more pronounced propagation observed in the experiments compared to FEA predictions. Furthermore, texture evolution was found to be a crucial factor affecting crack propagation, particularly with the development of the Goss texture component which is observed by electron backscattered diffraction analysis at bending points. The Goss texture hindered crack propagation, while the Brass texture allowed cracks to pass through. This phenomenon was consistent with both FEA and experimental observations. To mitigate edge crack formation and propagation, potential strategies involve promoting the formation of the Goss texture at the edge through alloy and process conditions, as well as implementing intermediate annealing to alleviate stress accumulation. These measures can enhance the overall quality and reliability of Al-Mg alloys during cross-rolling processes. In summary, understanding the mechanisms of defect formation and strain distribution in Al-Mg alloys during rolling processes is crucial for optimizing their mechanical properties. The findings of this study provide insights into the challenges associated with wave defects, strain localization, and crack propagation. Future research and optimization efforts should focus on implementing strategies to minimize defects and improve the overall quality of Al-Mg alloys in industrial applications.

Keywords: high Mg content Al-Mg alloy; Finite Element Analysis (FEA); electron backscattered diffraction (EBSD); cross-rolling; defect; Goss texture

1. Introduction

Lightweighting has been dealt with a significant objective, because the carbon emission should be reduced by improving fuel efficiency of vehicles[1,2]. Therefore, substituting from heavy metals, such as steels, copper alloys, etc., to lightweight materials like Al alloys, Mg alloys, carbon based materials. Among those substitutional candidate materials, Al-Mg alloys are recognized as the best materials, specifically in the area of body sheets for vehicles or sheets for battery packs of electric cars, because of its properties, which are high strength, good ductility, and ease of fabrication[1,2]. For these reasons, the Al-Mg alloys have been widely investigated, but there are several problems to be

 doi:10.20944/preprints202307.1095.v1

applied to the industrial area, such as low r-value, texture control, and stress corrosion cracking[3–10]. In order to solve these problems, the addition of Mg content has been suggested by several researchers. Mg addition is effective to control texture evolution, and increase r-value, and change grain boundary condition which is favorable to resist stress corrosion cracking.

Particularly, it was confirmed that Al-Mg alloys with high Mg content follow the brass-type texture evolution at cold rolling process by Cho et al.[8–11] According to the research8, the evolution of brass type texture was observed in Al-6Mg and -8Mg alloys, and it was confirmed that it was due to restriction of cross slip and acceleration of planar slip due to the high Mg content. However, it was shown that the addition of Mg content did not contribute to strain distribution and additional mechanical property improvement due to the absence of mechanical twin formation. Furthermore, high Mg content causes the Portevin Le-Chatelier effect and negative strain rate sensitivity effect12. These effects make irregular deformation of Al alloys. Therefore, another way to improve workability of Al-Mg alloys should be invented and investigated, not only controlling chemical composition.

Previous study conducted by Huh et al.[13,14], it was confirmed that the cross-rolling process is effective to randomize lattice orientation distributions, even though the annealing process is conducted after cross-rolling. Comparing between conventional cold-rolling and cross-rolling processes, cross-rolling accelerates brass-type texture evolution of aluminum alloys which is favorable for improving formability. Furthermore, for cross-rolling process is severe plastic deformation, high stored energy can be realized in the materials, which can be seeds for granular and small sized grains by recrystallization at annealing states15. As a result, the plastic anisotropy is effectively suppressed by the cross-rolling process. However, overall strain gradient during cross-rolling in Al-Mg alloys has not been investigated and discussed yet, and the defects which occur during cross-rolling have not been dealt by researchers.

The purpose of this study is to analyze the strain distribution and defects at normal cold-rolling and cross cold-rolling processes according to the strain mode change for Al alloy with high Mg content and the crack formation mechanism at the edge. In this study, the edge region of cross-rolled and normal rolled specimens in Al-6Mg alloy is investigated compared to the center region of rolled specimens and simulated by finite elements analysis (FEA). By FEA, the final shape of rolled specimens and strain distribution at deformation state and after deformation are estimated. And then, the defects of rolled specimens are examined by electron backscattered diffraction (EBSD) method.

2. Materials and Methods

In this study, an Al-6Mg plate with dimensions of 100mm x 100m x 2mm was chosen as a virtual specimen and real test specimen. In the virtual test of FEA, the real rolling test was simulated. Two virtual rollers were set to have 200mm of diameter and rotate at 6 rpm of angular velocity. The initial gap between the upper and lower rollers started from 2mm and gradually decreased to 1mm with 0.2mm decrement for each rolling process. Two different rolling processes had been set up: normal rolling and cross-rolling. For the normal rolling process, the rolling direction was retained as the specimen moved in one direction. However, the specimen for the cross-rolling was rotated 90° in clockwise when each rolling process was done. Overall experimental procedures are illustrated in Figure 1.

In the real rolling test, the homogenized Al-6Mg alloy was used. The chemical composition of the Al-6Mg alloy is 6.0-6.4 wt% Mg, 0.048 wt% Ca, with the balance being Al. The Al billets were machined into sheet samples with 100 mm width and 2 mm thickness for the rolling process. The diameter of the upper and lower rollers was 300 mm, and the speed of the rolls were 6 rpm. To investigate the strain mode effect, each sample was cold-rolled at room temperature. Some of them were conducted by conventional normal rolling, but the others were processed by cross-rolling. In the normal cold-rolling process, the rolling direction was retained while the sample was rotated clockwise by 90° with respect to the normal direction for each rolling pass in the cross cold-rolling process. In the cross-rolling process, the thickness of the sheets was reduced to 0.8 mm, corresponding to a reduction ratio of 60%. The thickness was reduced by 0.2 mm for each rolling pass.

The rolled samples were machined by electric discharge wire cutting machine (AD325L, Sodick, Japan). The observed plane was ground using SiC papers from #1000 to #4000 and 1 μm diamond suspension. Then, it was polished again by vibratory polisher (VibroMet, Buehler, U.S.A.) with 0.02 μm colloidal silica. The microstructure of those polished specimens was investigated using the EBSD

Preprints (www.preprints.org) | NOT PEER-REVIEWED | Posted: 17 July 2023 doi:10.20944/preprints202307.1095.v1

method. The EBSD data were acquired using a field emission scanning electron microscope (FE-SEM SU5000, Hitachi, Japan) equipped with an EBSD camera (Velocity Super, EDAX-Ametek, U.S.A.). To ensure the reliability of EBSD data, the measurement region was designated to be 1000 μm x 1000 μm and the step size is 1.0 μm. According to the collected EBSD data, inverse pole figure (IPF) maps, kernel average misorientation (KAM) data, and orientation maps were calculated and plotted by an orientation imaging microscopy (OIM) program version 8.5 (TSL OIM Analysis 8.5, EDAX-Ametek, U.S.A.). The observed planes of the specimens were transverse direction or rolling direction 2-the rolling direction after the first 90-degree clockwise turning of the specimens in the cross-rolling process-of the center of the specimens.

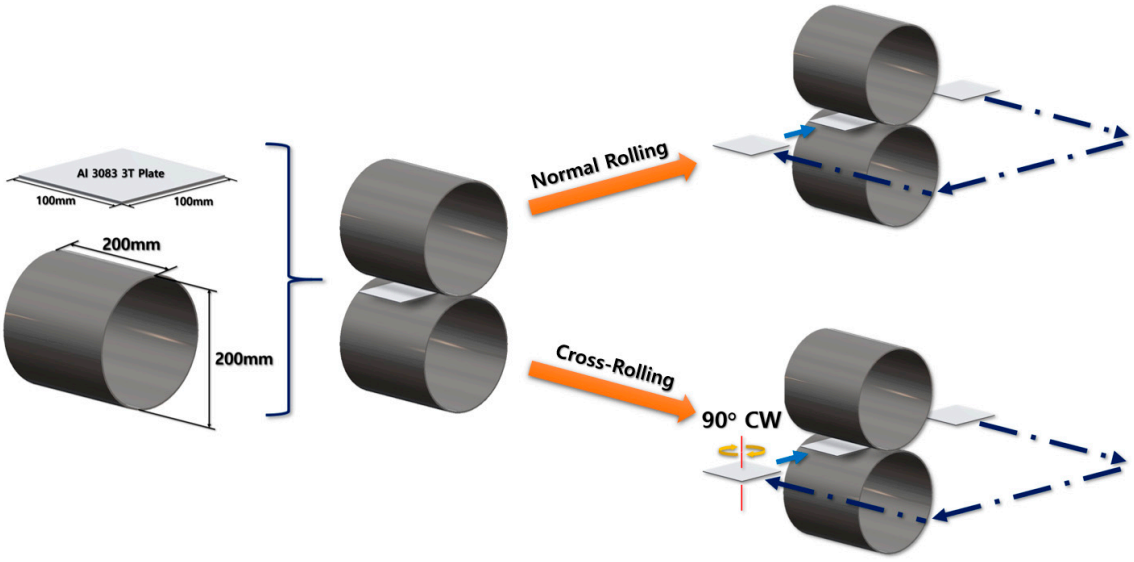

Figure 1. Schematic diagram of normal rolling and cross-rolling processes.

3. Methodology: Finite Element Analysis (FEA) via Abaqus

FEA for normal rolling and cross-rolling has been performed using Abaqus 2020. First, a specimen plate and a roller were modeled. Their dimensions were designed as mentioned in **Error! Reference source not found.**. The plate and the roller were defined to be deformable and discrete rigid respectively. Then, the material properties were set and applied to the specimen. Its specific property values are shown in Table 1–3.

Table 1. Material Properties of 5083 Al Alloy Applied in FEA(Density and Elasticity).

Material	Material Properties		
	Density [kg/mm^3]	Young's Modulus [MPa]	Poisson's Ratio
Al-6Mg	2.64e-6	70000	0.3

Table 2. Material Properties of Al-Mg Alloy Applied in FEA(Plasticity).

Data #	Material Properties	
	Yield Stress [MPa]	Plastic Strain
1	167	0
2	200	0.05
3	250	0.075

Preprints (www.preprints.org) | NOT PEER-REVIEWED | Posted: 17 July 2023 doi:10.20944/preprints202307.1095.v1

4	275	0.1
5	300	0.14
6	320	0.2
7	310	0.222

Table 3. Material Properties of Al-Mg Alloy Applied in FEA(Damage).

Johnson-Cook Damage Failure Parameters	
d1	0.0261
d2	0.263
d3	-0.349
d4	0.247
d5	16.8
Reference Strain Rate [s^{-1}]	1
Displacement at Failure [mm]	0.02

Material properties of Al-6Mg alloy relevant to density, elasticity and damage referred to Table 2. Johnson-Cook model parameters for Al-6Mg HI 16 and steel 4340 in LS-Dyna[16]. Plastic properties of the alloy were tabulated in Table 2 based on Figure 12. The displacement-strength curves of Al-6Mg, 6005A and 7N01 Al alloys welded joints[17].

There are various criterion models to define damage: Ductile, FLD, FLSD, Johnson-Cook, Maxe/Quade, Maxs/Quads, M-K, MSFLD, Shear, Hashin. In this study, Johnson-Cook damage criterion was selected because the rest of the models were unavailable or inappropriate for the cold-rolling situation. FLD and FLSD criteria were for necking situation of the metal sheet. Maxe/Quade and Maxs/Quads criteria were to predict damage initiation in cohesive elements where the cohesive layers are defined in terms of traction-separation. Shear criterion was only for shear models. Hashin damage model was not for ductile materials. Ductile, Johnson-Cook, M-K, and MSFLD damage criteria were chosen at the beginning. Among them, only Johon-Cook damage parameters for Al-6Mg could be easily obtained.

After finishing the material settings, all of the parts were properly placed in the assembly module to visualize the cold-rolling process as shown in Figure 1. The gap between the rollers was set at 1.8mm and reduced by 0.2mm for every rolling process.

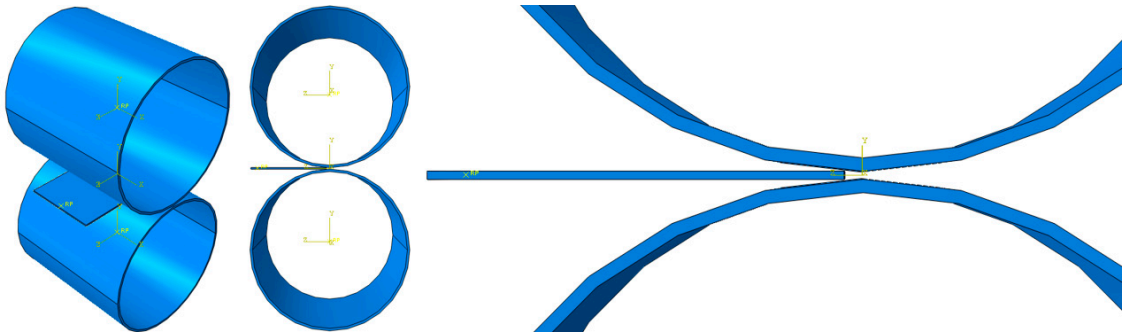

Figure 1. Assembly for cold-rolling FEA.

Each analysis has gone through two dynamic and explicit steps. The first step was a short step finished in 0.1s for the specimen to get close enough to the rollers. In this case, it was set to 0.03s after several attempts with different durations. The second step was for the actual cold-rolling process. It was set to 3s at the first rolling FEA and gradually extended up to 5s as the specimen was stretched through the rollers. The output was recorded in 200 evenly spaced time intervals for the second step duration.

Preprints (www.preprints.org) | NOT PEER-REVIEWED | Posted: 17 July 2023 doi:10.20944/preprints202307.1095.v1

According to Figure 2, reference points and 3-dimensional local coordinates were placed at the center of the rollers. For the reference points of the rollers, only rotational motion about the x-axis was allowed, and the other motions were fixed based on their local coordinates. Then, an angular velocity of 6rpm was applied to each roller. Since the Abaqus unit system requires the angular velocity in radians per second, the velocity value was converted into 0.63 rad/s. Eventually, the upper roller and the lower roller were set to have 0.63 rad/s and -0.63 rad/s of angular velocity according to the local coordinates.

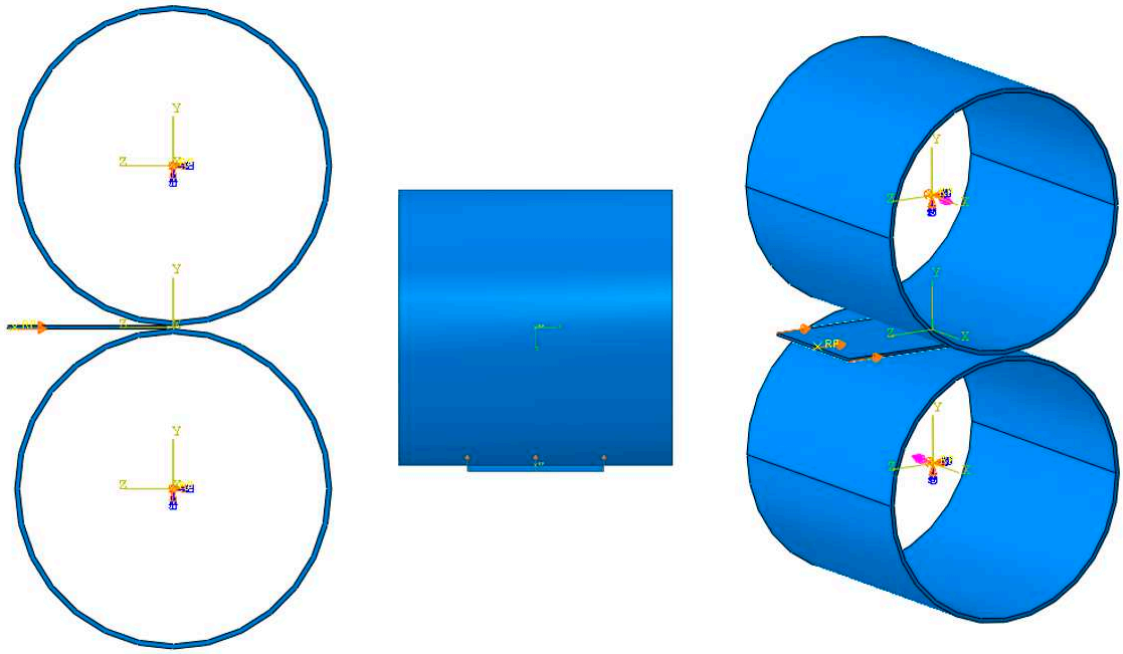

Figure 2. Load applied to the cold-rolling model.

Because the operator pushes the specimen toward the gap between the rollers, a displacement of 1mm was forced on the specimen surface where the operator pushes(Figure 2).

The rollers were coarsely auto-meshed regardless of the even distribution of the mesh using Abaqus auto-mesher function. Since the rollers were discretely rigid parts, it does not affect the analysis result as long as their rolling surfaces are circular enough. On the other side, the specimen plate was the main deformable model to be analyzed. The 2mm-thick specimen was finely sliced into 6 layers so that the result has enough precision to see how the plate deforms through the rolling process. It made the layer thickness be 0.333mm along the y-axis. The number of elements along the other axis was decided so that each element has a cubic shape as possible. Consequently, a specimen plate with $\mathbf{100mm \times 100 \times 2mm}$ dimesion was fully meshed and its element size was $\mathbf{0.384mm \times 0.333mm \times 0.384mm}$. The meshed parts are illustrated in Figure 3.

Preprints (www.preprints.org) | NOT PEER-REVIEWED | Posted: 17 July 2023 doi:10.20944/preprints202307.1095.v1

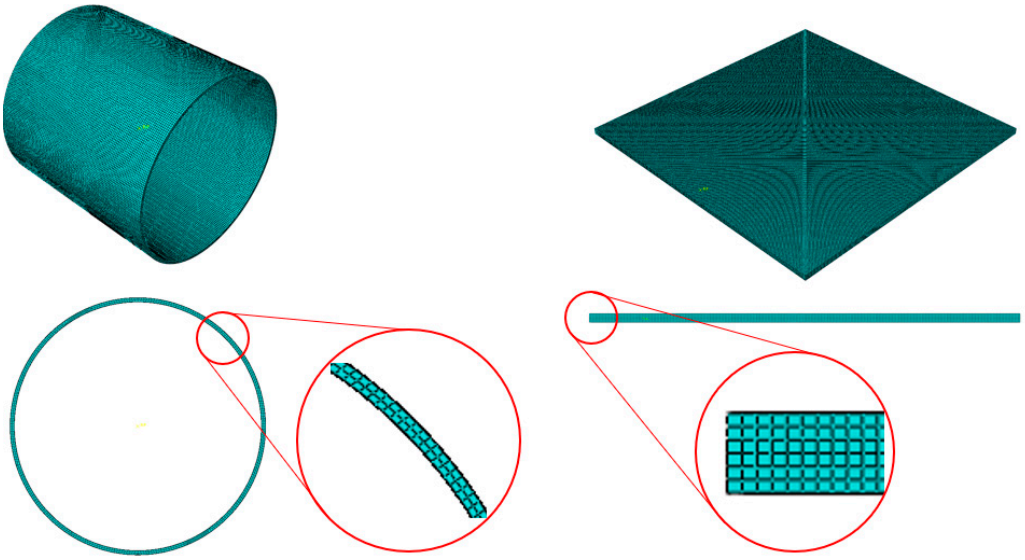

Figure 3. Meshed parts of the cold-rolling model.

The element type of the specimen part was C3D8R which means an 8-node linear brick, reduced integration and hourglass control. Additionally, its element library referred to explicit, and distortion control was deactivated to see drastic dimensional change by the rolling process. Besides, element deletion was activated considering the situation that a huge crack occurs and splits the plate apart.

4. Results

Figure 5 shows EBSD results of normal cold-rolled and cross-rolled specimens. Particularly, this figure indicates defects of surface and edge region of specimens. There are defects from rolling process, which are wavy edges, edge cracks, zipper cracks in the center of plate, and alligatoring. Among those known rolling defects, zipper cracks and edge cracks are identified in Al-Mg alloys with high Mg content. Particularly, the zipper cracks are shown after normal cold-rolling process, but in cross-rolling, edge cracks are strongly shown. These defects are identified by confidence index (CI) value which is calculated by EBSD OIM program. At the low CI value region, there is black, but at the high value, there is not. CI values are calculated during EBSD observation by intensity of Kikuchi line and eigenvalue of materials. Distortion of lattice, defects, or other factors affect the acceleration of low CI value. In this study, the formation of cracks makes CI value lowered.

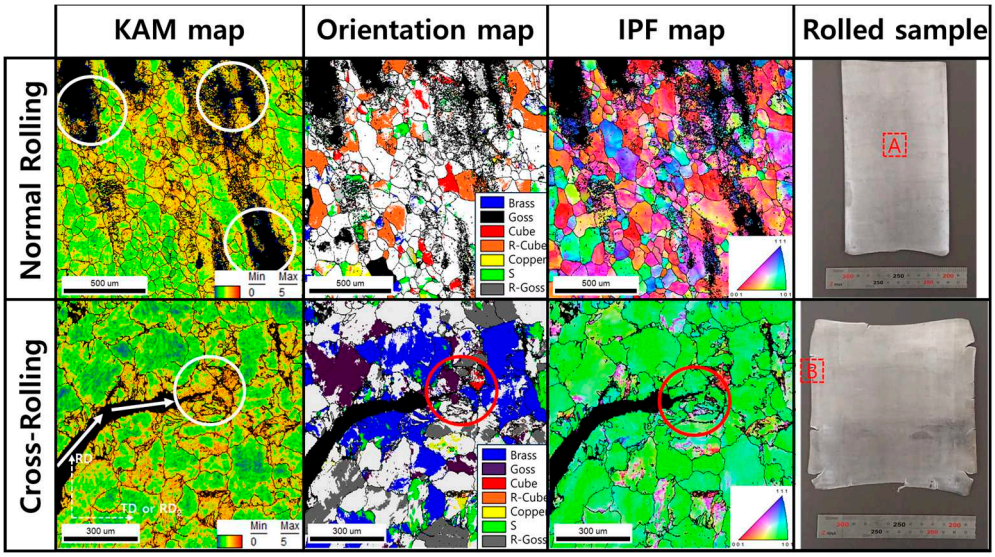

Figure 5. Normal rolled and cross-rolled EBSD results (KAM maps, Orientation maps, IPF maps, Measurement location which is shown in Rolled sample).

Preprints (www.preprints.org) | NOT PEER-REVIEWED | Posted: 17 July 2023 doi:10.20944/preprints202307.1095.v1

According to the KAM maps in Figure 5, the region around cracks has high value of KAM. The KAM value means the misorientation between adjacent points, which is observed by EBSD[8,11,12]. In other words, the KAM values are exhibited by formation of geometrical necessary dislocations which can be considered as stored energy. It can be figured out that high stored energy is related to forming crack and its propagation. The stored energy is also related to orientation evolution. Around cracks, there are oriented grains, such as rotated cube (R-cube) in normal rolling and Brass component in cross-rolling. The highly deformed region is oriented to ideal rolling texture component. The ideal rolling texture components are listed in Table 4.

Table 4. Ideal FCC rolling texture components (the orientations are indicated by Bunge's notation [18,19]).

Orientation	Miller indices	φ_1	Φ	φ_2
Cube	{001}<100>	45	0	45
Goss	{110}<001>	90	90	45
Brass	{110}<112>	55	90	45
Rotated Goss	{011}<011>	0	90	45
Rotated Cube	{001}<110>	0/90	0	45
Copper	{112}<111>	90	35	45
S	{123}<634>	59	37	63

FEA results of the first rolling process are illustrated below(**Error! Reference source not found.**6–9).

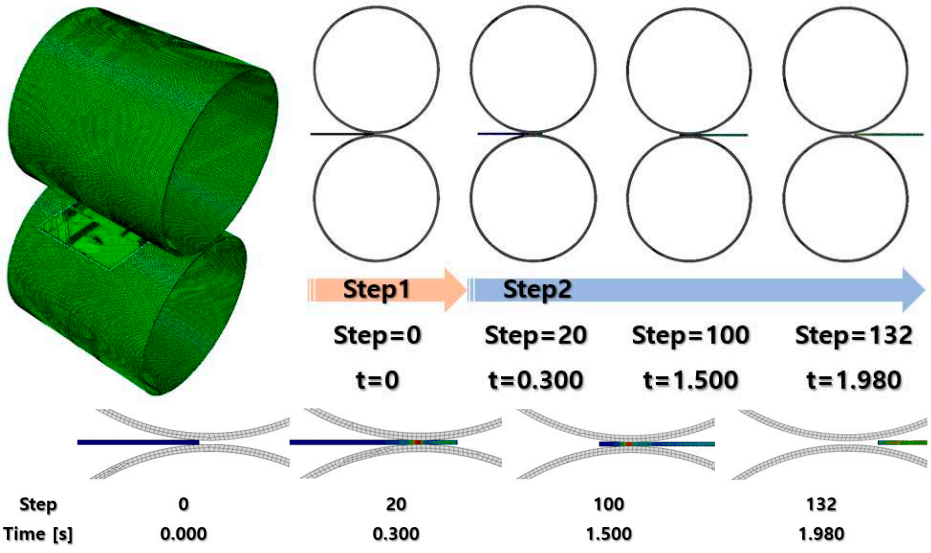

Figure 6. First rolling process result.

Preprints (www.preprints.org) | NOT PEER-REVIEWED | Posted: 17 July 2023 doi:10.20944/preprints202307.1095.v1

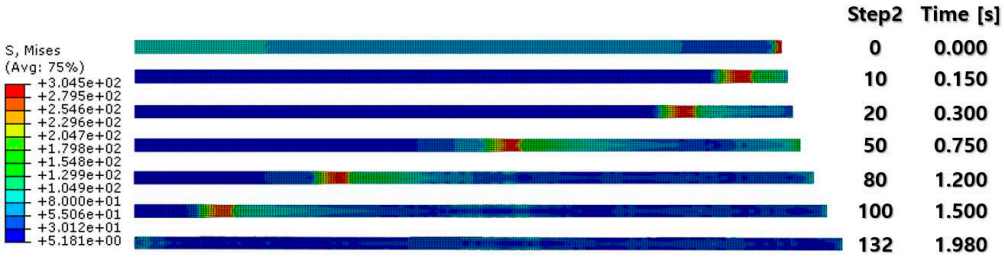

Figure 7. FEA result of first rolling process(side section view).

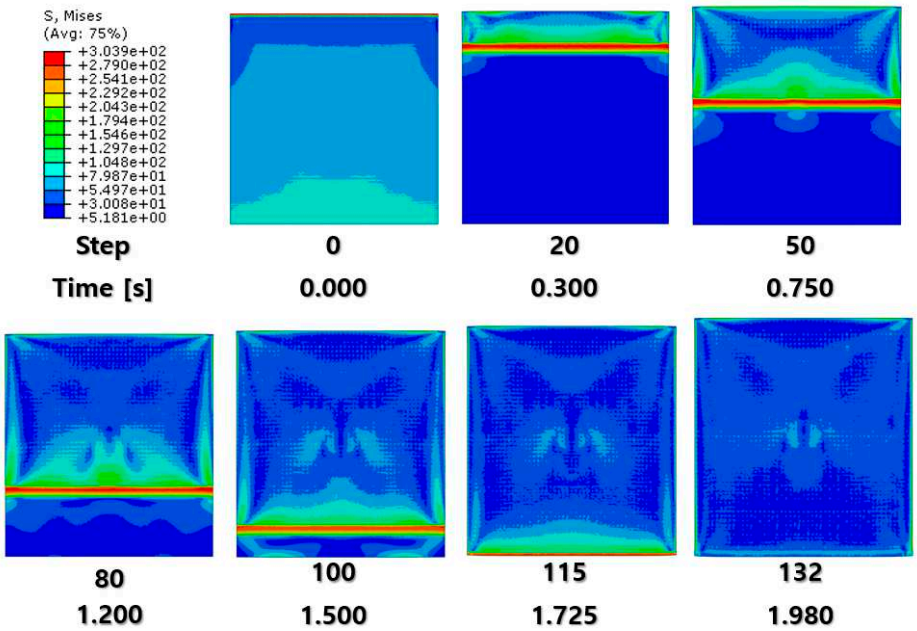

Figure 8. FEA result of first rolling process(top section view).

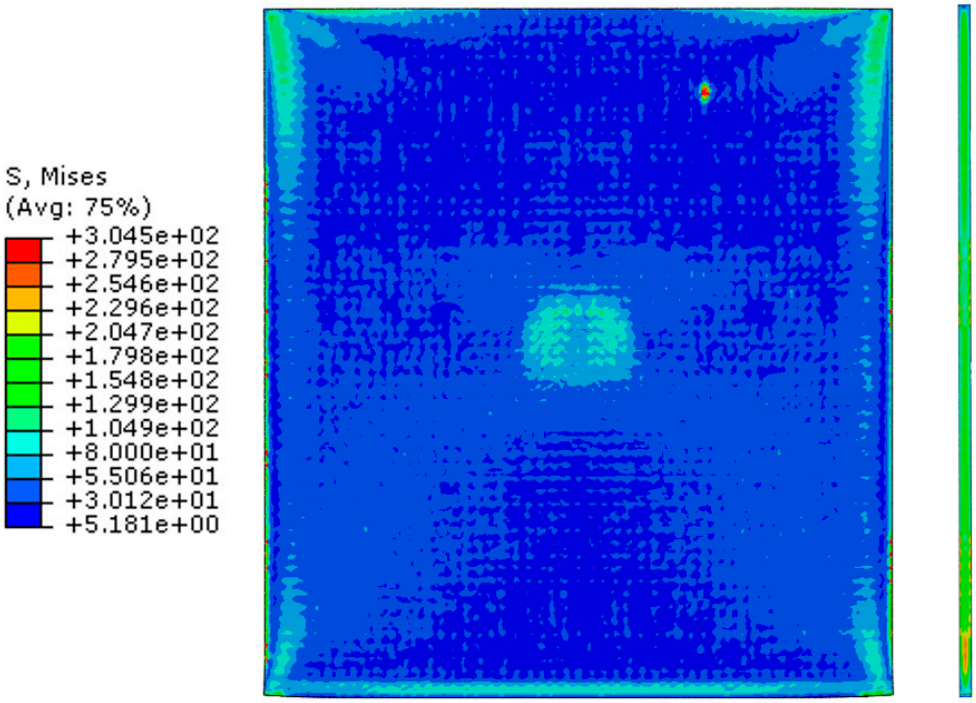

Figure 9. FEA result of first rolling process(external surfaces).

Error! Reference source not found.7 and 8 show section view of the specimen over time under the first cold-rolling process which machines a 2mm-thick aluminum alloy plate into a 1.8mm

Preprints (www.preprints.org) | NOT PEER-REVIEWED | Posted: 17 July 2023 doi:10.20944/preprints202307.1095.v1

thickness plate. According to the figures, as its thickness gets thinner through the tiny gaps between the rollers, over 300Mpa pressure is applied to the plate and stretches the specimen in its transitional direction. Moreover, it is observed that the residual stress after the high pressure over its yield strength is not stabilized and has the possibility to affect the machining quality of the successive cold-rolling processes. The external shape of the cold-rolled specimen is illustrated in Figure 9. It describes the concentration of the residual stress at each edge of the specimen with light colors. Some parts of them are excessively deformed and expressed as red spots – top right and both side edge of the specimen in top view(Figure 9).

The specimen after the first rolling process in Figure was gone through the next cold-rolling processes based on **Error! Reference source not found.** and explanation in **Error! Reference source not found.**. The thickness of the specimen was reduced by 0.8mm with 0.2mm decrement for each rolling process whose machining results are elaborated below(**Error! Reference source not found.**10–Figure 85).

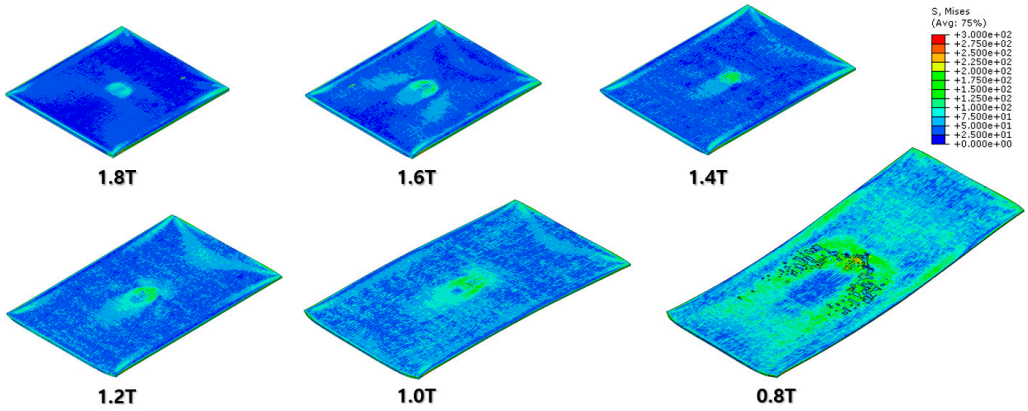

Figure 10. FEA result of normal cold-rolling results(Isometric).

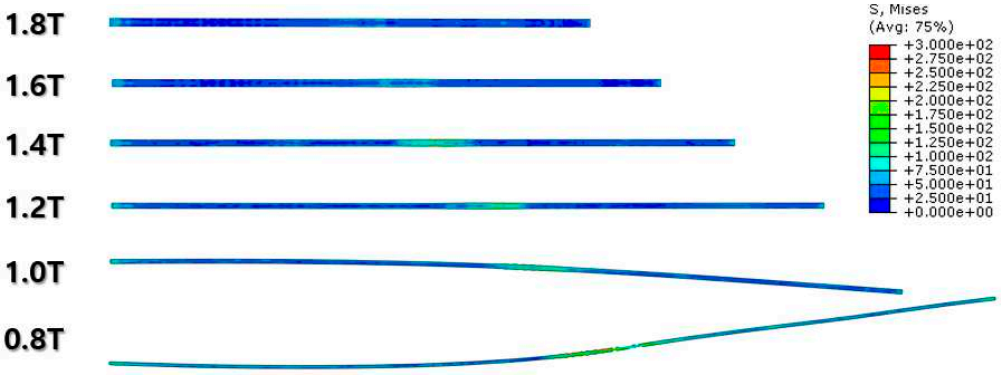

Figure 41. FEA result of normal cold-rolling results(Side section).

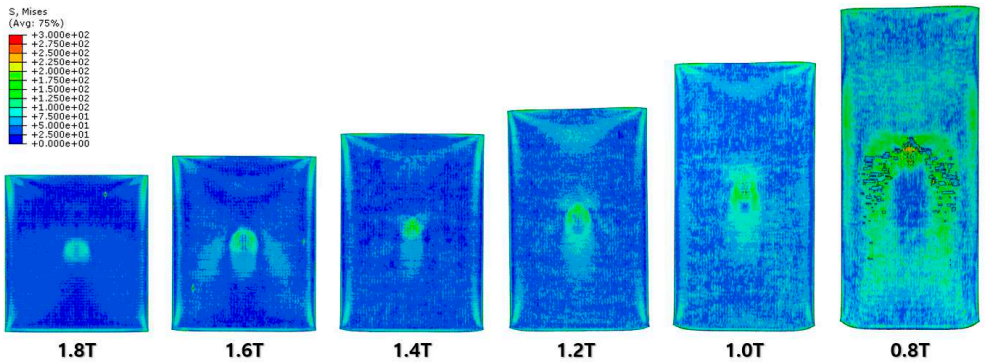

Figure 52. FEA result of normal cold-rolling results(Top).

Error! Reference source not found.10–Figure 85 show FEA results of normal rolling and cross rolling respectively. Both results are scaled in the same strength range from 000 MPa to 300 MPa.

Preprints (www.preprints.org) | NOT PEER-REVIEWED | Posted: 17 July 2023 doi:10.20944/preprints202307.1095.v1

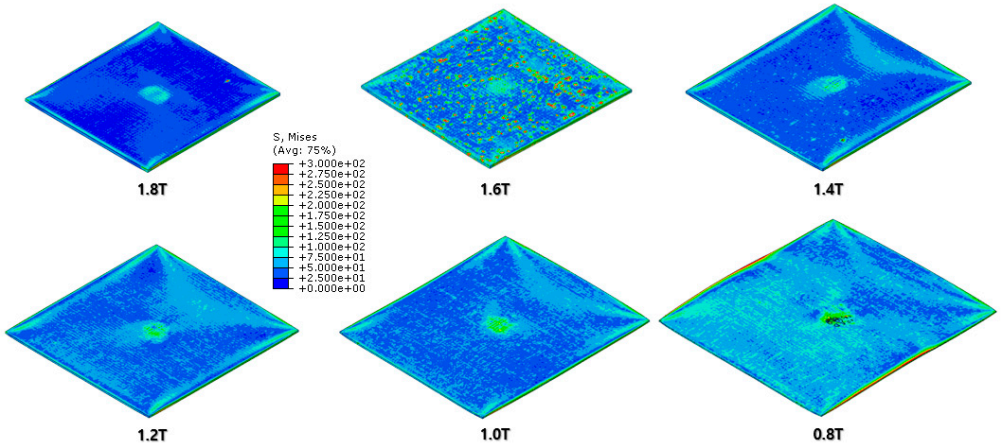

Figure 63. FEA result of cross cold-rolling results(Isometric).

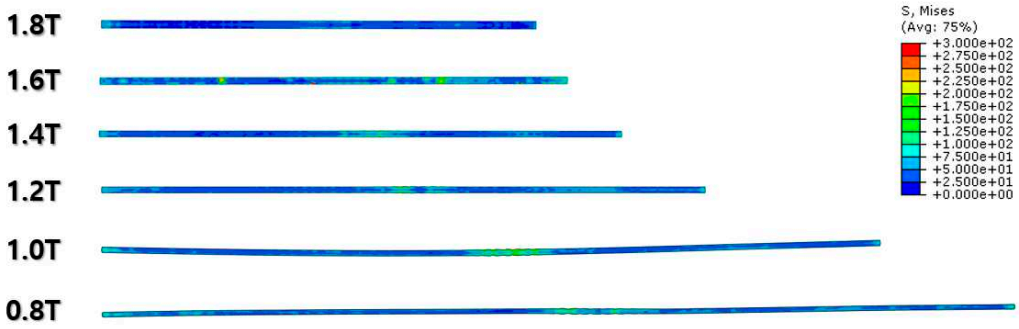

Figure 74. FEA result of cross cold-rolling results(Side section).

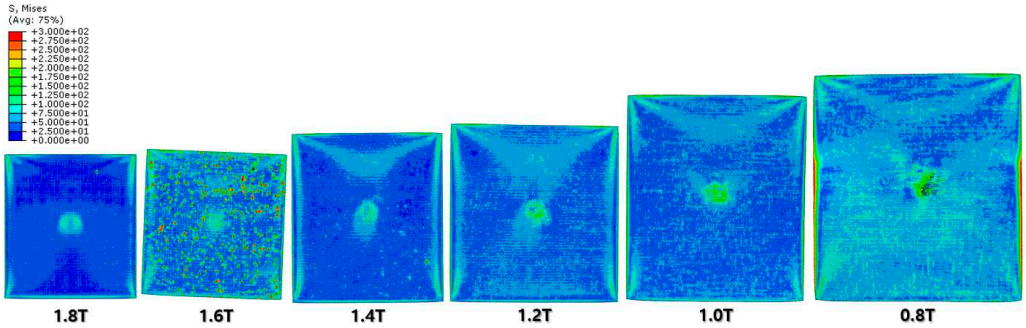

Figure 85. FEA result of cross cold-rolling results(Top).

According to the FEA results, normal rolling process stretches the specimen in single direction and remarkably changes original shape of the specimen while cross rolling process doesn't due to rotation of the rolling direction. Figure 52 and Figure 85 state that center and side edge of the specimen in rolling direction is under the largest pressure in overall cold-rolling process including both of normal and cross rolling methods. However, large amount of defects are detected in normal rolling process compared to the cross rolling as the specimen after normal rolling process should endure larger moment from its weight due to its longer length than one from the cross rolling process. More specific figures of the final FEA results from both rolling processes are illustrated below(Figure 96 and Figure 107).

Preprints (www.preprints.org) | NOT PEER-REVIEWED | Posted: 17 July 2023 doi:10.20944/preprints202307.1095.v1

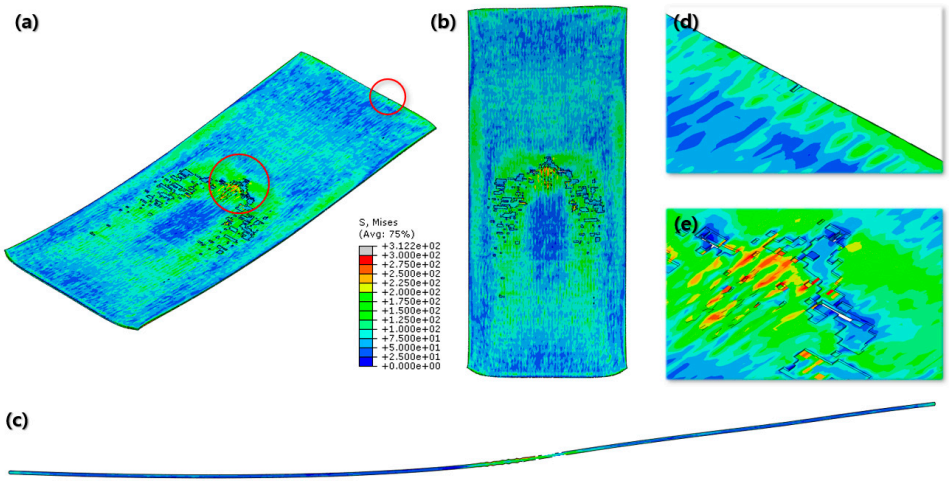

Figure 9. Final FEA result of normal cold-rolling process; Isometric view(a); Top view(b); Side section view(c); Crack at front edge(d); Defects at center(e).

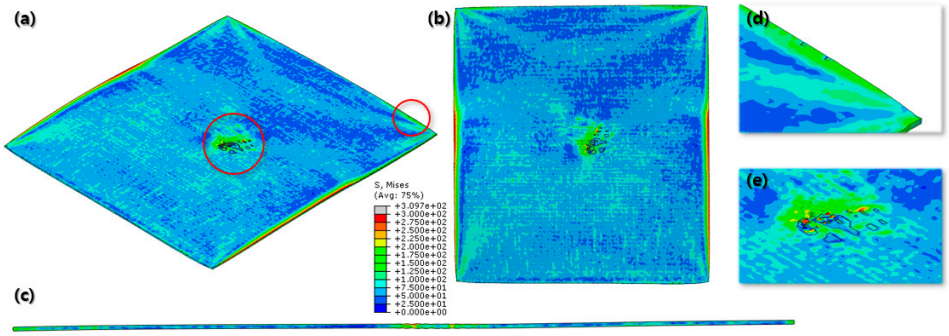

Figure 10. Final FEA result of cross cold-rolling process; Isometric view(a); Top view(b); Side section view(c); Cracks at front edge(d); Defects at center(e).

Both normal and cross rolling results show defects at front edge and center are created as strain excessively increases. As mentioned before, normal rolling result has more severe defects, even an hollow hole at center of the specimen due to its higher moment from its stretched length by the rolling method. When it comes to the defects at the front edge, result from the cross rolling process has more defects than the normal rolling result.

Even more details of the FEA results are described above(Figure 11). It shows the wrinkled side edge of the specimen after cross rolling which does not appear under normal rolling process. It is formed by 90 degree rotation of the specimen for each rolling which is the major difference between the normal and cross rolling processes. The wrinkly front and rear edges of the specimen strongly strained right before cracking from the previous rolling become side edges for the next rolling process as the specimen rotates 90 degree. The wrinkly side edges are stretched along the next rolling direction become even easier to get cracked during next cross rolling process as front and rear edges containing higher residual stress than the normal rolling process. Likewise, Figure 96 and Figure **10**7 show that specimen from cross rolling process has the red side edges which means higher stress than the one from the normal rolling process. According to (c) and (d) in Figure 118, (d) has more cracks than (c). Moreover, (d) from the normal rolling process shows rectangular corner from its original shape, but meanwhile, (c) from the cross-rolling process pinched-like corner because it was pressured over and over in the same rolling direction.

Preprints (www.preprints.org) | NOT PEER-REVIEWED | Posted: 17 July 2023 doi:10.20944/preprints202307.1095.v1

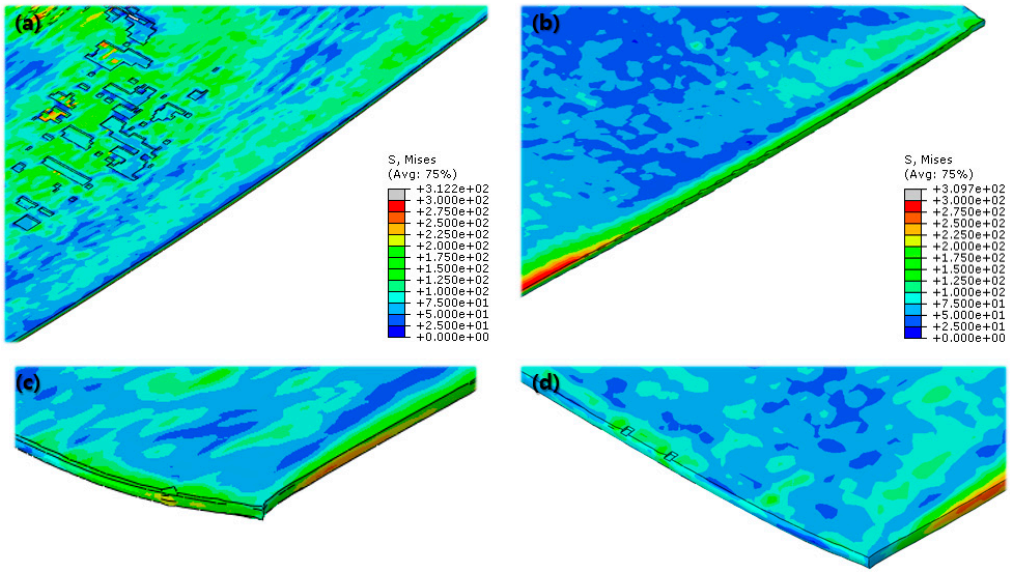

Figure 11. Comparison of the Final FEA results from normal and cross cold-rolling processes; Side edge after normal cold-rolling process(a); Side edge after cross cold-rolling process(b); End corner after normal cold-rolling process(c); End corner after cross cold-rolling process(d).

5. Discussion

Al-Mg alloys are widely used materials that offer a combination of lightweight properties and enhanced strength[1,2]. Among the various processing methods for Al-Mg alloys, conventional normal rolling and cross rolling are commonly employed. These two methods have a notable influence on defect formation and strain distribution during the processing of the alloy[13–15,20]. Understanding and controlling these defects and strain distributions are crucial as they can significantly affect the final mechanical properties of the alloy. Hence, this paper aims to investigate the defect formation and strain distribution in high Mg content Al-Mg alloys during both normal rolling and cross rolling processes[21–25]. By doing so, we seek to comprehend the underlying mechanisms responsible for defect formation during the alloy's processing and propose strategies to mitigate these issues. Additionally, gaining insights into the strain distribution of the alloy will assist in deriving optimal processing conditions.

In the FEA conducted to predict the strain distribution, only the influence of the processing itself was considered, excluding the effects of thermal energy generation and segregation of elements. In the case of normal cold-rolling, the formation of wave defects and zipper cracks due to strain localization near the center was predicted, clearly indicating an uneven distribution of strain. Experimental results also support the formation of zipper cracks, and based on the results of KAM analysis and texture formation, it is inferred that crack formation and propagation are caused by the concentration of shear strains. KAM indicates geometrical necessary dislocation existence[26], so as high KAM regions mean highly dislocations piled-up regions. In Figure. 16, the region of high value of strain is shown. The region was detected by EBSD, and which is shown as Figure. 5. In this figure, the formed zipper cracks are shown, and around these cracks, high KAM values are clearly shown. Around these cracks, grains are highly oriented rotated cube orientation component. The component is evolved by shear strain. In other words, the concentration of shear strain which is caused by rolling makes high stored energy, which is indicated by KAM, and texture evolution, as well as crack formation and propagation.

The wave defects observed by the FEA were observed in the actual tested specimens, albeit to a lesser extent due to the small size of the specimens, making it difficult to quantify the variations. However, if applied to actual mass production processes, it is expected that the defective rate will significantly increase due to wave defects. In particular, when the rolling process is applied to specialized shape processing rather than flat rolling, the issue of wave defects is expected to become more pronounced. In conclusion, the FEA results reveal the presence of wave defects and strain localization-induced zipper cracks in normal cold rolling. These defects were confirmed in the

 doi:10.20944/preprints202307.1095.v1

experimental samples, albeit with limited quantification due to the sample size. Nevertheless, if implemented in real-world mass production processes, the detrimental effects of wave defects are expected to increase the defect rate significantly. It is especially anticipated that specialized shape processing using the rolling process will exacerbate the issue of wave defects[21]. Further research and optimization efforts are required to address these challenges and enhance the overall quality of Al-Mg alloys during rolling processes.

In contrast to normal rolling, FEA results show a relatively uniform distribution of strain in the cross-rolling process (Figure 15). Furthermore, the influence of wave defects was predicted to be minimal. These findings were consistent with the results obtained from the actual experiments. It suggests that the nature of the cross-rolling process itself does not induce significant wave defects. However, strain concentration was observed at the edge and center regions, with a predicted formation of zipper cracks at the center. In the actual experiments, the formation of edge cracks was observed due to stress concentration at the edges. The formation of cracks in the experiments was more pronounced and exhibited more significant propagation compared to the predictions from FEA. Overall, the cross-rolling process demonstrates certain advantages over normal rolling in terms of strain distribution and the reduced influence of wave defects. However, the potential for crack formation, particularly at the center and edge regions, should not be overlooked. Further investigations and optimization strategies are necessary to address these concerns and enhance the overall quality of Al-Mg alloys during the cross-rolling process.

Upon examining the formation and propagation of cracks in the cross-rolling process, it was observed that cracks exhibited a change in direction at specific locations (Figure 5). Upon closer inspection of these crack bending points, it was evident that stress concentration played a role, typically aiding in crack propagation[27,28]. However, it appeared that the crack propagation was impeded. The reason for this hindrance can be attributed to texture evolution. Analyzing the grain orientations at the bending points revealed the development of the Goss texture component. Among the ideal rolling texture components for FCC metals, which includes orientations that form the deformation texture, Goss, Brass, Copper, and S components are present. Specifically, the orientations belonging to the α-fiber (ND//{110}) category correspond to Goss and Brass. While Brass allows cracks to pass through, Goss was found to act as an orientation component that impedes crack propagation[4,29–32]. This phenomenon was also observed in the actual experimental results.

Applying this principle, several approaches can be considered to mitigate the formation and propagation of edge cracks. Firstly, establishing alloy and process conditions that promote the formation of the Goss texture at the edge region can be a viable solution. Given that Goss orientation hinders crack propagation, it can serve as an efficient mechanism. Secondly, implementing an intermediate annealing process can alleviate the stress accumulation at the edge, effectively preventing crack formation at its origin[33–35].

In summary, the investigation revealed that cracks in the cross-rolling process exhibited directional changes at specific points, likely due to stress concentration. The hindrance of crack propagation was found to be associated with the development of the Goss texture at these bending points. To address edge crack formation and propagation, potential solutions involve promoting Goss texture formation through alloy and process conditions, as well as introducing intermediate annealing to alleviate stress accumulation at the edge. Further research and optimization of these approaches are essential to enhance the quality and reliability of Al-Mg alloys during cross-rolling processes.

6. Conclusions

In this study, the high Mg content Al-Mg alloy is investigated in order to identify the probability of defects at normal cold-rolling and cross-rolling processes. FEA is conducted to predict defects caused by the rolling processes. Specimens were taken from the regions where defects were anticipated, and EBSD analysis was conducted. The results of the EBSD analysis were then compared and analyzed in relation to the FEA findings. In both FEA and EBSD results, the application of normal rolling showed the formation of wave defects and zipper cracks. In the case of cross-rolling, wave defects were absent, but the formation of edge cracks and zipper cracks was observed. Understanding these issues can be beneficial when implementing these processes in actual mass production. Further research is needed to address these challenges, such as investigating intermediate annealing or

exploring additional strategies to maximize the Goss texture component. These studies will contribute to resolving the identified problems and improving the effectiveness of the rolling process in real-world industrial applications.

Funding: This study was supported by the grant titled with "Development of a precise formability prediction method of refractory alloys for manufacturing high-performance aerospace parts (No. KITECH UR-23-0013)".

Data Availability Statement: We encourage all authors of articles published in MDPI journals to share their research data. In this section, please provide details regarding where data supporting reported results can be found, including links to publicly archived datasets analyzed or generated during the study. Where no new data were created, or where data is unavailable due to privacy or ethical restrictions, a statement is still required. Suggested Data Availability Statements are available in section "MDPI Research Data Policies" at https://www.mdpi.com/ethics.

Acknowledgments: The authors are grateful to Dr. Jinkyu Lee and Dr. Sunki Kim of NICE LMS, who provided the Al-Mg alloys.

Conflicts of Interest: The authors declare no conflict of interest.

References

1. Benedyk JC. Aluminum alloys for lightweight automotive structures. In: *Materials, Design and Manufacturing for Lightweight Vehicles*. Elsevier; 2010:79-113.Author 1, A.; Author 2, B. Title of the chapter. In *Book Title*, 2nd ed.; Editor 1, A., Editor 2, B., Eds.; Publisher: Publisher Location, Country, 2007; Volume 3, pp. 154–196.
2. Zhang R, Knight SP, Holtz RL, Goswami R, Davies CHJ, Birbilis N. A survey of sensitization in 5xxx series aluminum alloys. *Corrosion*. 2016;72(2):144-159.Author 1, A.B.
3. Ailinei II, Galatanu SV, Marsavina L. Influence of anisotropy on the cold bending of S600MC sheet metal. *Eng Fail Anal*. 2022;137:106206.
4. Leffers T, Ray RK. The brass-type texture and its deviation from the copper-type texture. *Prog Mater Sci*. 2009;54(3):351-396. doi:10.1016/j.pmatsci.2008.09.002
5. Beausir B, Scharnweber J, Jaschinski J, Brokmeier HG, Oertel CG, Skrotzki W. Plastic anisotropy of ultrafine grained aluminium alloys produced by accumulative roll bonding. *Mater Sci Eng A*. 2010;527(13-14):3271-3278.
6. Bunge HJ, Grzesik D, Ahrndt G, Schulze M. The relation between preferred orientation and the Lankford parameter r of plastic anisotropy. *Arch Für Eisenhüttenwes*. 1981;52(10):407-411.
7. Lee KM, Huh MY, Park S, Engler O. Effect of texture components on the Lankford parameters in ferritic stainless steel sheets. *ISIJ Int*. 2012;52(3):522-529.
8. Cho CH, Son K, Cho H. Experimental analysis of deformation texture evolutions in pure Cu, Cu-37Zn, Al-6Mg, and −8Mg alloys at cold-rolling processes. *J Alloys Compd*. 2023;934:167879. doi:10.1016/j.jallcom.2022.167879
9. Cho CH, Son HW, Hyun SK. Effect of Mg content on shear texture evolution at variable processing conditions in Al–Mg alloys. *J Alloys Compd*. 2020;825:153927.
10. Cho CH, Lee JW, Son KT, Hyun SK. Strain rate effects on microstructure and texture evolution in cold-sheared Al-6 Mg alloys during low-temperature annealing. *J Alloys Compd*. 2021;889:161630.
11. Cho CH, Son KT, Lee JC, Kim SK, Yoon YO, Hyun SK. Effect of the Mg contents on the annealing mechanism and shear texture of Al–Mg alloys. *Mater Sci Eng A*. 2020;786:139471.
12. Cho CH, Son HW, Lee JC, Son KT, Lee JW, Hyun SK. Effects of high Mg content and processing parameters on Portevin-Le Chatelier and negative strain rate sensitivity effects in Al–Mg alloys. *Mater Sci Eng A*. 2020;779:139151.
13. Huh MY, Cho SY, Engler O. Randomization of the annealing texture in aluminum 5182 sheet by cross-rolling. *Mater Sci Eng A*. 2001;315(1):35-46. doi:10.1016/S0921-5093(01)01207-2
14. Huh MY, Engler O, Raabe D. On the Influence of Cross-Rolling on Shear Band Formation and Texture Evolution in Low Carbon Steel Sheets. *Texture Stress Microstruct*. NaN/NaN/NaN;24:225-237. doi:10.1155/TSM.24.225
15. Liu W, Li X, Meng X. Effect of pseudo cross-rolling on the recrystallization texture of a continuous cast Al–Mg alloy. *Scr Mater*. 2009;60(9):768-771. doi:10.1016/j.scriptamat.2009.01.015
16. Rashed A, Yazdani M, Babaluo AA, Hajizadeh Parvin P. Investigation on high-velocity impact performance of multi-layered alumina ceramic armors with polymeric interlayers. *J Compos Mater*. 2016;50(25):3561-3576.
17. Wu L, Yang B, Han X, et al. The microstructure and mechanical properties of 5083, 6005A and 7N01 aluminum alloy gas metal arc-welded joints for high-speed train: a comparative study. *Metals*. 2022;12(2):213.
18. Zhou Y, Toth LS, Neale KW. On the stability of the ideal orientations of rolling textures for fcc polycrystals. *Acta Metall Mater*. 1992;40(11):3179-3193.

19. Suwas S, Ray RK. *Crystallographic Texture of Materials*. Springer; 2014.
20. KIM SH, KIM DG, KANG HG, HUH MY, LEE JS, ENGLER O. EVOLUTION OF STRAIN STATES AND TEXTURES IN AA 5052 SHEET DURING CROSS-ROLL ROLLING. *Int J Mod Phys B*. Published online January 25, 2012. doi:10.1142/S0217979208051650
21. Liang C, Li S, Liang J, Li J. Method for Controlling Edge Wave Defects of Parts during Roll Forming of High-Strength Steel. *Metals*. 2021;12(1):53.
22. Li Q, Lovell MR, Slaughter W, Tagavi K. Investigation of the morphology of internal defects in cross wedge rolling. *J Mater Process Technol*. 2002;125:248-257.
23. Liu G, Zhong Z, Shen Z. Influence of reduction distribution on internal defects during cross-wedge-rolling process. *Procedia Eng*. 2014;81:263-267.
24. Yu H liang, Tieu K, Lu C, Deng G yu, Liu X hua. Occurrence of surface defects on strips during hot rolling process by FEM. *Int J Adv Manuf Technol*. 2013;67:1161-1170.
25. Dodd B, Boddington P. The causes of edge cracking in cold rolling. *J Mech Work Technol*. 1980;3(3-4):239-252.
26. Rui SS, Niu LS, Shi HJ, Wei S, Tasan CC. Diffraction-based misorientation mapping: A continuum mechanics description. *J Mech Phys Solids*. 2019;133:103709.
27. Freiman SW, Mulville DR, Mast PW. Crack propagation studies in brittle materials. *J Mater Sci*. 1973;8:1527-1533.
28. Yılmaz O, Bleyer J, Molinari JF. Influence of heterogeneities on crack propagation. *Int J Fract*. 2018;209:77-90.
29. Li F, Liu Z, Wu W, et al. Enhanced fatigue crack propagation resistance of Al-Cu-Mg alloy by intensifying Goss texture and refining Goss grains. *Mater Sci Eng A*. 2017;679:204-214.
30. Wu W, Liu Z, Hu Y, et al. Goss texture intensity effect on fatigue crack propagation resistance in an Al-Cu-Mg alloy. *J Alloys Compd*. 2018;730:318-326.
31. Li F, Liu Z, Wu W, et al. On the role of texture in governing fatigue crack propagation behavior of 2524 aluminum alloy. *Mater Sci Eng A*. 2016;669:367-378.
32. Son K, Kassner ME, Lee TK, Lee JW. Mg effect on the cryogenic temperature toughness of Al-Mg alloys. *Mater Des*. 2022;224:111336.
33. Yu HL, Lu C, Tieu AK, Li HJ, Godbole A, Zhang SH. Special rolling techniques for improvement of mechanical properties of ultrafine-grained metal sheets: a review. *Adv Eng Mater*. 2016;18(5):754-769.
34. Harries DR, Smith GC. Fatigue damage and crack formation in pure aluminium. *J Inst Met*. 1959;88.
35. Polák J. On the role of point defects in fatigue crack initiation. *Mater Sci Eng*. 1987;92:71-80.